Sound propagation in SF_6 near the critical point*

David S. Cannell† and Dror Sarid‡
Department of Physics, and Quantum Institute, University of California at Santa Barbara, Santa Barbara, California 93106
(Received 25 July 1974)

We have used the acoustic-beam probing technique of Gordon and Cohen to measure the speed and attenuation of 36-MHz sound in sulfur hexafluoride near its critical point. The measurements were made along the critical isochore. We have also analyzed all existing sound-speed and attenuation data on the critical isochore in the temperature range $0.1 \leq T - T_c \leq 10.0$ °C. We find that it is possible to model all available data with a frequency-dependent viscosity, involving a slightly modified form of the frequency dependence calculated by Kawasaki using the mode-mode coupling approach of Kadanoff and Swift, together with a single relaxation to account for energy exchange with the vibrational states. We also find that a single-relaxation model involving no critical contribution is not adequate to account for the data.

INTRODUCTION

Measurement of the frequency and temperature dependence of the sound speed and attenuation in a pure fluid near its gas-liquid critical point is an excellent method for determining its dynamic behavior. Because of the extremely high values of attenuation encountered near the critical point the acoustic-beam probing technique of Gordon and Cohen[1] offers an ideal method of making such measurements. As Kadanoff and Swift,[2] and Kawasaki[3] have shown by their calculations, the dynamic behavior of critical systems is intimately connected with the anomalous changes which occur in the static properties of such systems, as the critical point is approached. In a pure fluid, sound propagation is influenced markedly by the divergence of the adiabatic compressibility K_S. As a result of this divergence the speed of very-low-frequency sound approaches zero near the critical point; however, the velocity of higher-frequency sound is less affected. This can be understood physically in the following manner. The divergence of the various thermodynamic susceptibilities can be traced to the fact that the spontaneous density fluctuations which occur in any medium, and are normally correlated over a distance of only a few angstroms, become correlated over distances as large as thousands of angstroms near the critical point. Since the equilibrium correlation is a function of density and temperature, any compression requires the transport of matter over distances of the order of the correlation range to restore local thermodynamic equilibrium. Since such transport requires an ever longer time as the critical point is approached, a compression must occur at an ever lower frequency in order to correspond to the static compressibility. Compressions which occur in times less than the time required for the restoration of equilibrium are accompanied by greater pressure increases than would have occurred if the same compression had been carried out quasistatically. This effect results in a substantial dispersion in the speed of sound near the critical point. This dispersion is accompanied by a remarkable rise in attenuation due to the fact that sound-wave energy is used during the compression to modify the fluid correlation and is not all returned during the expansion. These effects are very similar to the dispersion and attenuation which occur in all fluids possessing structural relaxation. In the case of the critical fluid the important time scale is set by the time required for mass transport to occur over a distance of one correlation length. Since the primary transport mechanism in a critical fluid is thermal diffusion, as witnessed by the great intensity of the Rayleigh scattering, the relevant time is[2] $(\Lambda/\rho_0 C_P \xi^2)^{-1}$, where Λ is the thermal conductivity, ρ_0 the density, C_P the constant-pressure specific heat, and ξ the long-range correlation length. Because of the rapid variation of Λ, ξ, and C_P the corresponding angular relaxation frequency

$$\omega_R = \Lambda/\rho_0 C_P \xi^2 \tag{1}$$

changes by orders of magnitude as the critical point is approached.

In the case of a monatomic fluid, such as xenon, Kawasaki has calculated an expression for the complex frequency-dependent viscosity, which is directly applicable to a determination of the expected dispersion and attenuation as functions of temperature when the critical point is approached.[3] As one of the authors (D.S.C.) has pointed out,[4] the equations used by Kawasaki in relating the viscosity to the sound speed and attenuation are inadequate when the total dispersion is a significant fraction of the low-frequency sound speed. In addition the relationship between wave-vector-dependent sound speed and attenuation as determined by

light scattering, and a frequency-dependent viscosity is quite complicated, and differs from the case of driven sound waves. The extraction of accurate information regarding the frequency dependence of the viscosity from measurements of the Rayleigh-Brillouin spectrum can be extremely difficult in general.[5] Garland and co-workers[6-8] have made extensive ultrasonic measurements in xenon and have analyzed their own results as well as light scattering data[5,9] in terms of Kawasaki's expression for the viscosity. In so doing they derived and used a more accurate connection between the viscosity and the sound speed and attenuation than the one originally given by Kawasaki. In treating light scattering data they used the Brillouin splittings and linewidths to deduce the wave-vector-dependent attenuation and sound speed, and compared these results to those predicted by Kawasaki's expressions for the frequency-dependent attenuation and sound speed at the Brillouin frequency. In principle one should use the frequency-dependent viscosity to compute the expected light scattering spectrum and compare the result with the observed spectrum; however, the difference is expected to be substantial only when the Brillouin half-width is comparable to the Brillouin splitting divided by 2π.[4] As a result of their work and that of Cummins and Swinney[9] it appears that the dispersion and attenuation observed in xenon are reasonably well accounted for. Recently Eden and Swinney[10] have used a heterodyne light scattering technique to measure dispersion and attenuation in xenon in the frequency range from 2.4 to 24 MHz and also find that Kawasaki's calculations correspond well to their data. In all of this work, however, it is found that at any temperature the observed attenuation at high frequencies is nearly equal to the maximum value obtained from Kawasaki's calculation, which occurs at the sound-wave angular frequency of $14\omega_R$. For this reason, in our own analysis we have used the maximum, rather than the calculated values of the attenuation, for $\omega \geq 14\omega_R$.

In the case of SF_6, sound propagation is complicated by the existence of internal degrees of freedom capable of storing energy. The responsible states are the vibrational modes, which have quanta comparable to k_BT and exchange energy slowly with the translational motion. The rotational states contribute the classical value $3k_B/2$ per molecule to the heat capacity, since the rotational quanta are very small compared to k_BT; and since the rotational states reach equilibrium very rapidly they are not responsible for dispersion of sound, at accessible frequencies. Although both light scattering[11] and ultrasonic measurements[12,13] have been made near the critical point of SF_6 they had not been subjected to extensive analysis[14] since the frequency regime from 1 to 130 MHz remained unexplored. For this reason we have measured both the speed and attenuation of 36-MHz sound in SF_6 in the vicinity of its critical point. We have also collected and analyzed all existing data taken on the critical isochore employing a frequency-dependent viscosity to account both for the slow exchange of energy between the vibrational degrees of freedom and the translational motion as well as the effects of the critical point. As will be shown, it is quite straightforward to use the measured values of attenuation and sound speed to compute the real and imaginary parts of the viscosity as a function of frequency, which may then be compared directly to the predictions of any model or theory of interest. We have found this to be a great advantage in a system as complicated as SF_6. In the following sections of the paper we describe the experimental method used in our sound-speed and attenuation measurements and present our results together with all other data available on the critical isochore. We next derive the necessary connections between the experimentally observed quantities and the real and imaginary parts of the frequency-dependent viscosity $b(\omega)$, and use all available data to deduce $b(\omega)$ as a function of temperature. We then assemble all of the thermodynamic parameters necessary to evaluate Kawasaki's expression for $b(\omega)$. In the data-analysis section we show that it is not possible to account for all of the data in terms of a single relaxation due to energy exchange with the vibrational states, but that very good agreement can be obtained by including the critical contribution to the viscosity.

EXPERIMENTAL METHOD

The method employed was the acoustic-beam probing technique of Gordon and Cohen.[1] Figure 1 is a schematic diagram of the experimental setup. Light from a He-Ne laser operating in the TEM_{00} mode was spatially filtered, collimated, and chopped at 1 KHz. It then passed through a half-silvered mirror M_1. One of the resulting beams was allowed to fall on a photodiode D_1 which generated a reference signal for the lock-in amplifier. The other beam passed through a counterrotating window W_1, entered the cell through window W_2, and was specularly reflected from the interface between the SF_6 and the face of the fused-quartz buffer rod. It was then reflected by mirror M_2, exited through window W_2, passed again through the counterrotating window W_1, was reflected by mirror M_1, and was focused upon a high speed, back-biased, photodiode D_2. The purpose of the counterrotating window was to prevent the beam

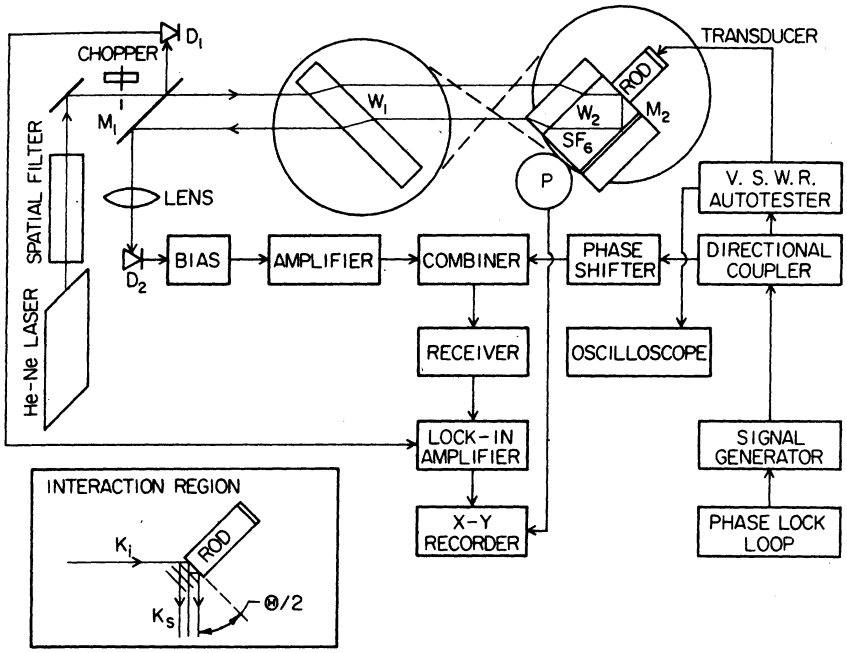

FIG. 1. Schematic diagram of the acoustic-beam probing apparatus.

from moving across the face of the buffer rod when the cell was rotated. A 5-MHz quartz transducer operating at its seventh harmonic was used to inject an acoustic wave into the SF_6 from the face of the buffer rod. In this manner a small fraction of the incident light beam could be scattered from the acoustic wave before being reflected by the rod. In addition, as shown by the inset in Fig. 1, a small fraction of the light beam was backscattered by the sound wave after the light had already been reflected from the buffer rod, and this backscattered light was rereflected from the face of the rod. The acoustic wave can scatter light only when its wave vector $\vec{K}$ is oriented so as to satisfy the Bragg condition $\vec{k}_i \pm \vec{K} = \vec{k}_s$, where $\vec{k}_i$ and $\vec{k}_s$ are the wave vectors of the light incident upon and scattered from the acoustic wave, respectively. By rotating the cell about an axis passing through the center of the face of the buffer rod while monitoring the amplitude of the light scattered from the acoustic wave it was possible to determine accurately the angle at which maximum scattering occurred. This is given by $2nk_0 \sin(\Theta/2) = |\vec{K}|$, where n is the index of refraction of the SF_6 and k_0 is the magnitude of the wave vector of the incident light in vacuo. The angle $\Theta/2$ is as shown in the inset. The above condition holds because the fractional energy gain or loss suffered by the light upon being scattered from the acoustic wave is negligible. In this manner it was possible to determine the wave vector of the acoustic wave, and since its frequency was already known, this served to determine the sound speed.

As shown in Ref. 1 a damped acoustic wave with an amplitude proportional to $e^{-\alpha x}$ results in a scattering amplitude with an angular dependence of the form $\{[2nk_0 \sin(\Theta/2) - |\vec{K}|]^2 + \alpha^2\}^{-1}$. Thus by measuring the signal amplitude as a function of angle in the vicinity of the Bragg angle it was possible to determine the amplitude attenuation coefficient α. Since the acoustic attenuation resulted in appreciable scattering over an angular range as large as 12° it was necessary to correct the measured signal amplitude for the angular dependence of the reflectivity of the face of the rod. Since the angular spread caused by diffraction of the light leaving the face of the rod was negligible compared to the spread caused by acoustic attenuation, this effect was neglected. An additional possible source of spurious angular spread in the scattered light is that due to the diffraction angle of the acoustic wave in the SF_6. Since our transducer had a transverse dimension of 0.4 cm, and the sound velocity in SF_6 is $\sim 10^4$ cm/sec this angle was less than 10^{-3} rad and was thus negligible. In practice a potentiometer P was driven by the rotating table used to turn the cell. The potentiometer divided a stable voltage, providing the x signal for an x-y recorder, which was then calibrated in degrees of table rotation. The y signal was provided by the amplitude of the scattered light signal itself.

In order to detect the light which had been scattered by the acoustic wave it was necessary to heterodyne beat it against the light which had been reflected from the face of the rod, because the

scattered and reflected beams were superimposed. The light which was scattered by the acoustic wave before encountering the rod was Doppler shifted upward in frequency by an amount equal to the acoustic-wave frequency while the light scattered by the acoustic wave after having been reflected from the rod was Doppler shifted down in frequency by a like amount. In beating on the face of the photodiode D_2, with the light which had only been reflected and not scattered, each of these beams produced a component in the photocurrent at the frequency of the acoustic wave and this component was detected using a receiver tuned to 36 MHz. It is important to correct for the fact that the 36-MHz beat notes produced by these two beams are 180° out of phase, but do not cancel completely because one of them is reduced in amplitude by having undergone two reflections from the buffer rod.[1] By chopping the incident light and using a lock-in amplifier to detect the difference in the output of the receiver with and without the incident light beam on, it was possible to discriminate very effectively against spurious signals which are generated by the rf equipment used to drive the transducer, and picked up by the sensitive receiving equipment. A much more thorough and technical description of both the electronic and optical details of this technique is to be found in Ref. 1, to which we refer the interested reader.

The scattering cell was constructed of beryllium copper, with optical-glass windows sealed into recesses using indium gaskets. One of the windows was chromed on the inside and served as a mirror. The buffer rod was inserted through a hole in the side of the cell and held in place by epoxy applied from outside the cell. In order to prevent the critical fluid from contacting epoxy, the rod was soldered to the cell on the inside using indium as solder. The temperature was controlled to 1 m °C using the first stage of an extremely accurate (±15 μ°C) temperature controller which has been described elsewhere.[15] The density was adjusted to within 0.1% of the critical density by using a cathetometer to measure the position of the liquid-vapor interface as a function of temperature below the critical temperature T_c. These measurements also served to determine T_c. All temperature measurements were made relative to T_c using a thermistor as sensor. Comparison of the thermistor and an accurate glass-stem thermometer gave T_c as 45.5°C ± 0.1°C. Neither the optical nor the acoustic power exceeded 1 mW, and the observed sound speed and attenuation were independent of these powers.

In Table I we present our measured values of the sound speed and attenuation per wavelength, $\alpha\lambda$. In addition we have collected all other data available in the same temperature range and display it as well. Since the Brillouin scattering data are not obtained at constant frequency we give the actual frequencies calculated using the relationship $\omega = CK$, where C is the Brillouin sound speed and K the scattering wave vector, which does remain constant. We computed the values of $\alpha\lambda$ given for the 360-MHz data directly from the published values[11] of the Brillouin half-widths $\Delta\nu_{1/2}$, using the relationship $\alpha\lambda = 2\pi\Delta\nu_{1/2}/f_B$, where f_B is the Brillouin frequency. The 600-kHz data were

TABLE I. Velocity C in cm/sec and attenuation per wavelength $\alpha\lambda$ at various temperatures and frequencies. (Values in parentheses are estimated.)

		$T - T_c$ (°C)						
Frequency		0.1	0.5	1.0	2.0	5.0	10.0	Ref.
2 kHz	C	5798	6326	6600	6918	7412	(7864)	13
	$\alpha\lambda$							
600 kHz	C	6150	6380	6620	6930	7424	(7876)	12
	$\alpha\lambda$	0.213	0.095	0.048	0.022	(0.020)	(0.020)	
1 MHz	C	6270	6510	6730	7050	7612	8064	13
	$\alpha\lambda$	0.37	0.23	0.15	(~0.1)	(~0.1)	(~0.1)	
36 MHz	C	7700	7800	7986	8184	9000	9500	This
	$\alpha\lambda$	1.36	1.35	1.34	1.32	1.28	1.2	work
~130 MHz	C		9400	9400	9600	10500	11600	11
	$\alpha\lambda$							
	f (MHz)		130	130	133	145	160	
~360 MHz	C	10200	10300	10400	10680	11300	12250	11
	$\alpha\lambda$	0.58	0.53	0.51	0.5	0.45	0.41	
	f (MHz)	360	363	367	377	399	432	

taken directly from the tables published in Ref. 12. The 2-kHz data were taken from the adiabatic compressibility data of Ref. 13 using the relationship $C = 1/(\rho_0 K_S)^{1/2}$ to compute C. In so doing we used a density ρ_0 of 0.70 g/cm^3, which is the density used by the authors in computing K_S from their measured values of C. The values of C obtained in this manner do not agree exactly with the values shown in Ref. 13 for $T - T_c \leq 2°$C, but the difference is slight. We used the compressibility because it was presented over a wider temperature range. In all other calculations we used a density of 0.737 g/cm^3. In collecting the data of other authors we took points from the smooth curves they had drawn through their data.

THEORY

The dispersion equation for driven sound in a medium obeying the linearized Navier-Stokes equation and the ordinary heat transport equation can be written[16]

$$\omega^2/\vec{K}\cdot\vec{K} = C_0^2 + ab(\omega)\vec{K}\cdot\vec{K} - i\omega[a + b(\omega) - C_0^2 a\vec{K}\cdot\vec{K}/\gamma\omega^2], \quad (2)$$

where $a = \Lambda/\rho_0 C_V$ is assumed to be frequency independent, and $b(\omega) = (1/\rho_0)[\frac{4}{3}\eta_s(\omega) + \eta_v(\omega)]$, where $\eta_s(\omega)$ and $\eta_v(\omega)$ are the frequency dependent shear and volume viscosities, respectively. $\vec{K}$ is the wave vector of the sound wave, ω its angular frequency, C_0 the zero-frequency sound speed, and $\gamma = C_P/C_V$. For a driven wave which is damped in space we can write $\vec{K} = \hat{n}(k + i\alpha)$, where $\hat{n}$ is a unit vector in the direction of propagation. In this case the phase velocity $C(\omega)$ of a sound wave of angular frequency ω is given by

$$C(\omega) \equiv \omega/k, \quad (3)$$

while its amplitude attenuation per wavelength $\alpha\lambda(\omega)$ is given by

$$\alpha\lambda(\omega) = 2\pi\alpha/k. \quad (4)$$

An experimental measurement of the sound speed and attenuation at a given frequency serves to determine k and α, which can then be used in Eq. (2) to calculate $b(\omega)$ at that frequency, provided that C_0, γ, and a are known. If necessary Eq. (2) can be solved exactly for the real and imaginary parts of $b(\omega)$; however, it is often the case that the terms involving a are small compared to $\omega b(\omega)$. If so the solutions take the relatively simple form

$$\omega\,\mathrm{Im}b(\omega) = C^2(\omega)\frac{1 - (\alpha\lambda/2\pi)^2}{[1 + (\alpha\lambda/2\pi)^2]^2} - C_0^2 \quad (5)$$

and

$$\omega\,\mathrm{Re}b(\omega) = \frac{\alpha\lambda(\omega)}{\pi}\frac{C^2(\omega)}{[1 + (\alpha\lambda/2\pi)^2]^2}. \quad (6)$$

In the event that $3(\alpha\lambda/2\pi)^2 \ll 1$ Eq. (5) reduces to

$$\omega\,\mathrm{Im}b(\omega) \simeq C^2 - C_0^2, \quad (7)$$

while if $2(\alpha\lambda/2\pi)^2 \ll 1$, Eq. (6) reduces to

$$\omega\,\mathrm{Re}b(\omega) \simeq [\alpha\lambda(\omega)/\pi]C^2(\omega). \quad (8)$$

If, in addition, the condition $C(\omega) - C_0 \ll C_0$ holds, then Eq. (7) further reduces to

$$\omega\,\mathrm{Im}b(\omega) \simeq 2C_0[C(\omega) - C_0]. \quad (9)$$

Equation (9) was used by Kawasaki[3] to relate $b(\omega)$ to $C(\omega) - C_0$, while he used Eq. (8) with $C(\omega)$ replaced by C_0 to compute $\alpha\lambda(\omega)$.

We have used Eqs. (5) and (6) and the data given in Table I to compute $\omega\,\mathrm{Re}b(\omega)$ and $\omega\,\mathrm{Im}b(\omega)$ at six different temperatures above T_c. When necessary we used the exact solutions to Eq. (2) rather than Eqs. (5) and (6), but the difference in the calculated values of $b(\omega)$ never exceeded 5%. It was only for the 360-MHz data that the classical contribution to the attenuation from $\Lambda/\rho_0 C_V$ was at all significant. Tables II and III give the results of the exact calculation as well as theoretical results calculated from a model to be described later. We present the experimental results in this manner because it is a convenient summary of the data and may easily be compared to the values predicted by theory. The tables also give, for each temperature and frequency, the values of the reduced frequency ω^* and the quantities $dJ(\omega^*)$ and $dI(\omega^*)$ defined below. As mentioned earlier, for values of $\omega^* > 7$, the values of $dI(\omega^*)$ listed are the maximum values assumed by $dI(\omega^*)$ and not the actual values.

Kawasaki has calculated both $\omega\,\mathrm{Re}b(\omega)$ and $\omega\,\mathrm{Im}b(\omega)$ for a fluid near its critical point. Taking the real and imaginary parts of Eq. (3.10) of Ref. 3, we obtain

$$\omega\,\mathrm{Re}b(\omega) = \frac{k_B T^3}{\pi^2\rho_0^3 C_V^2}\left(\frac{\partial P}{\partial T}\right)_V^2 \xi^{-1}\left(\frac{\partial \xi^{-1}}{\partial T}\right)_S^2 I(\omega^*) \quad (10)$$

and

$$\omega\,\mathrm{Im}b(\omega) = \frac{k_B T^3}{\pi^2\rho_0^3 C_V^2}\left(\frac{\partial P}{\partial T}\right)_V^2 \xi^{-1}\left(\frac{\partial \xi^{-1}}{\partial T}\right)_S^2 J(\omega^*), \quad (11)$$

where

$$I(\omega^*) = \int_0^\infty dx\,\frac{x^2}{(1+x^2)^2}\,\frac{\omega^* K(x)}{\omega^{*2} + K^2(x)} \quad (12)$$

and

$$J(\omega^*) = \int_0^\infty dx\,\frac{x^2}{(1+x^2)^2}\,\frac{\omega^{*2}}{\omega^{*2} + K^2(x)}. \quad (13)$$

In the above expressions k_B is Boltzmann's constant, T the absolute temperature, P the pressure, V the volume, and S the entropy. $K(x)$ is $3/4[1 + x^2 + (x^3 - x^{-1})\tan^{-1}x]$, and

TABLE II. Experimental and theoretical values of ω Imb (ω) in 10^6 cm^2/sec^2 at various temperatures and frequencies, and the values of b_1 in 10^6 cm^2/sec^2.

Frequency		$T-T_c$ (°C) 0.1	0.5	1.0	2.0	5.0	10.0
600 kHz	ω^*	7.39	0.226	0.053	0.012	1.5×10^{-3}	3.1×10^{-4}
	Expt.	4.07	0.66	0.26	0.16	0.18	0.19
	Fit	3.08	0.46	0.004	0.004	0.005	0.006
	dJ (ω^*)	3.07	0.45	0.00	0.00	0.00	0.00
1 MHz	ω^*	12.3	0.376	0.088	0.019	2.5×10^{-3}	5.2×10^{-4}
	Expt.	5.29	2.19	1.66	1.80	2.96	3.14
	Fit	3.56	0.69	0.23	0.01	0.01	0.02
	dJ (ω^*)	3.55	0.68	0.24	0.00	0.00	0.00
36 MHz	ω^*	443	13.5	3.18	0.70	0.09	0.02
	Expt.	17.9	12.9	12.1	10.8	16.6	19.1
	Fit	18.2	15.5	14.0	12.8	13.6	16.5
	dJ (ω^*)	6.2	4.2	2.8	1.2	0.3	0.0
~130 MHz	ω^*	1600	48.9	11.5	2.59	0.36	0.08
	Expt.		44.1	40.5	39.9	50.0	66.3
	Fit	54.7	50.7	49.4	49.8	56.7	72.4
	dJ (ω^*)	6.7	5.6	4.4	2.8	0.7	0.2
	f (MHz)	130	130	130	133	145	160
~360 MHZ	ω^*	4430	136	32.5	7.33	1.00	0.23
	Expt.	67.7	63.7	62.4	64.0	70.7	86.3
	Fit	68.3	64.2	62.9	63.9	70.1	85.8
	dJ (ω^*)	6.9	6.7	5.4	4.3	1.5	0.4
	f (MHz)	360	363	367	377	399	432
b_1	(fit)	64	60	60	62	71	88
b_1	(single relaxation)	21	32	40	50	58	50

TABLE III. Experimental and theoretical values of ω Reb (ω) in 10^6 cm^2/sec^2 for various temperatures and frequencies.

Frequency		$T-T_c$ (°C) 0.1	0.5	1.0	2.0	5.0	10.0
600 kHz	Expt.	2.56	1.23	0.67	0.34	0.35	0.39
	Fit	1.99	1.21	0.73	0.54	0.57	0.71
	dI (ω^*)	1.47	0.72	0.24	0.04	0.00	0.00
1 MHz	Expt.	4.59	3.10	2.16	1.58	1.84	2.07
	Fit	2.33	1.67	1.14	0.94	0.95	1.20
	dI (ω^*)	1.47	0.86	0.33	0.11	0.00	0.00
36 MHz	Expt.	23.3	23.8	24.8	25.7	30.3	32.0
	Fit	26.7	25.4	25.5	25.9	28.4	34.7
	dI (ω^*)	1.5	1.7	1.8	1.4	0.4	0.1
~130 MHz	Expt.	...	...	...	...	...	...
	Fit	30.2	28.7	28.9	29.5	31.2	35.4
	dI (ω^*)	1.5	1.7	1.9	1.9	1.0	0.3
~360 MHz	Expt.	18.0	16.9	16.7	17.3	17.6	19.0
	Fit	17.2	16.0	16.6	17.0	17.7	19.1
	dI (ω^*)	1.5	1.7	1.9	2.0	1.5	0.8
Expected relaxation frequency (MHz)		50	56	60	65	68	65

$$\omega^* = \omega/2\omega_R . \tag{14}$$

The extra factors of ρ_0 in our equations are due to the fact that our heat capacities are given per unit mass while those of Ref. 3 are given per unit volume. Garland and co-workers have calculated $I(\omega^*)$ and $J(\omega^*)$ and we have used their results. Swinney has pointed out[17] that the above expressions for $I(\omega^*)$ and $J(\omega^*)$ are exact only when the background contribution to the thermal conductivity is negligible compared to the critical part, which is not necessarily the case in SF_6. His calculations also show, however, that the values of $I(\omega^*)$ and $J(\omega^*)$ calculated from Eqs. (12) and (13) differ by at most 20% from the exact results. For this reason we have used the values given by Eden *et al.*[7]

In order to calculate the prefactor of $I(\omega^*)$ in Eq. (10) and of $J(\omega^*)$ in Eq. (11), which we denote by d, it is necessary to know C_V, $(\partial P/\partial T)_V$, and ξ as functions of the temperature along the critical isochore, and to evaluate ω^*, $\Lambda/\rho_0 C_P$ must be known as well. In the next section we evaluate these quantities, before analyzing the data.

DATA ANALYSIS

We begin by discussing the methods used to obtain the values of C_V, $(\partial P/\partial T)_V$, and ξ which we used to evaluate the prefactor d. Since directly measured values of C_V are not available we were forced to calculate C_V from measured values of the zero-frequency sound speed C_0, using the thermodynamic relationship[18]

$$\rho_0 C_V = \frac{T(\partial P/\partial T)_V^2}{\rho_0 C_0^2 - 1/K_T} \text{ erg/cm}^3\,^\circ\text{C}, \tag{15}$$

where K_T is the isothermal compressibility. In evaluating Eq. (15) we used the values of C_0 measured by Fritsch and Carome[13] at a frequency of 2 kHz, which have been presented in Table I, and calculated K_T from the equation

$$K_T = 1.26\times10^{-9}\left(\frac{T-T_c}{T_c}\right)^{-1.235} \text{ cm}^2/\text{dyn},$$

which is the best fit to the values measured by Feke *et al.*[19] These values of K_T agree to within experimental error with the measurements of Puglielli and Ford[20] over the entire temperature range of interest to us. Since we needed to know $(\partial P/\partial T)_V$ over a 10°C range and it has been measured by Feke *et al.*[19] over a range of 2.4°C only, we used the Martin-Hou equation for the pressure as a function of temperature and differentiated it to obtain $(\partial P/\partial T)_V$. The parameters entering the Martin-Hou equation have been carefully evaluated for SF_6 in the critical region, and the pressures thus calculated agree with great accuracy with the measured values over a wide range of density and temperature.[21] In the region where $(\partial P/\partial T)_V$ was measured by Feke *et al.*[19] the values calculated from the Martin-Hou equation agreed with their results to within 6%; however, an attempt to extend the fit they found to $(\partial P/\partial T)_V$ as a function of temperature along the isochore, to temperatures more than 4°C above T_c resulted in disagreement with the results calculated from the Martin-Hou equation. The values of ξ we used were obtained from preliminary measurements we have made in SF_6 using a technique described previously.[22] They agree well with values previously measured by Puglielli and Ford.[20] In order to calculate values for ω^* from the experimental frequencies we used values of $\Lambda/\rho_0 C_P$ taken from Feke *et al.*,[19] and our own values of ξ. We calculated $a \equiv \Lambda/\rho_0 C_V$ from $\Lambda/\rho_0 C_P$ using $C_P/C_V = K_T/K_S = \gamma$. In Table IV we present, for six different temperatures, the values of $(\partial P/\partial T)_V$, C_V, $\Lambda/\rho_0 C_P$, ξ, and γ used in all our calculations. The value for C_V at $T - T_c = 10$°C

TABLE IV. Values for the thermodynamic parameters used in the text as functions of temperature. (Values in parentheses are extrapolated or depend upon extrapolations.)

Thermodynamic parameters	$T-T_c$ (°C) 0.1	0.5	1.0	2.0	5.0	10.0
$\left(\frac{\partial P}{\partial T}\right)_V$ (10^5 dyn/cm^2 °C)	8.43	8.43	8.43	8.44	8.45	8.46
C_V (10^7 erg/g °C)	1.241	1.055	0.984	0.917	0.875	(.923)
$\Lambda/\rho_0 C_P$ (10^{-6} cm^2/sec)	2.0	8.5	15	28.5	(69)	(137)
ξ (Å)	280	101	65	42	24	15
γ	628	102	47	22	8	4
d (10^6 cm^2/sec^2)	9.6	11.3	12.2	13.3	(13.7)	(12.1)

was obtained by extrapolating the measured value of the zero-frequency sound speed from $T-T_c = 5.8°C$, while the values of $\Lambda/\rho_0 C_P$ at $T-T_c = 5$ and 10°C were obtained by extrapolating from $T-T_c = 2.5°C$. Fortunately the results of our analysis are quite insensitive to these quantities for $T-T_c \geq 5°C$. Table IV also gives the calculated values of

$$d \equiv \frac{k_B T^3}{\pi^2 \rho_0^3 C_V^2} \left(\frac{\partial P}{\partial T}\right)_V^2 \xi^{-1} \left(\frac{\partial \xi^{-1}}{\partial T}\right)_S^2 . \tag{16}$$

In evaluating $(\partial \xi^{-1}/\partial T)_S$ we used the fact that the critical density is very nearly the density at which ξ assumes its maximum value as a function of density at any given temperature above T_c. Thus $(\partial \xi^{-1}/\partial T)_S = (\partial \xi^{-1}/\partial T)_\rho$ at the critical density, a fact which has been used by previous workers.

We first calculated the differences between the experimentally determined values for $\omega \mathrm{Re} b(\omega)$ and $\omega \mathrm{Im} b(\omega)$, and the values calculated from Eqs. (10) and (11). We attempted to fit these differences to equations of the form

$$\omega \mathrm{Re} b_1(\omega) = \frac{b_1 \omega \tau}{1+\omega^2\tau^2} + \omega b_0 \tag{17}$$

and

$$\omega \mathrm{Im} b_1(\omega) = \frac{b_1 \omega^2 \tau^2}{1+\omega^2\tau^2} , \tag{18}$$

which has the form of a single relaxation in the viscosity. Here $b_0 = (1/\rho_0)(\frac{4}{3}\eta_{S0} + \eta_{V0})$ is the nonrelaxing part of the viscosity. We used[23] $\eta_{S0} = 4.25 \times 10^{-4}$ dyn sec/cm^2 and estimated η_{V0}, the nonrelaxing part of the volume viscosity as $\approx \eta_{S0}$. We found it possible to accurately fit all of the data in this manner. The next to last line in Table II gives the values of b_1 used in this fit. A relaxation frequency $f_\tau = 1/2\pi\tau$ of 75 MHz was found at all temperatures. The quantities $dJ(\omega^*)$ and $dI(\omega^*)$ listed in Tables II and III are the critical contributions to $\omega \mathrm{Im} b(\omega)$ and $\omega \mathrm{Re} b(\omega)$, respectively. Since we have used the maximum value of $I(\omega^*)$ for $\omega^* > 7$, these values represent an upper limit on the critical contribution to $\omega \mathrm{Re} b(\omega)$.

There are three minor discrepancies between the data and the fit which deserve comment. The fit does not account for the slight dispersion in the sound speed between the 2-kHz and 1-MHz data of Fritsch and Carome. This dispersion persists quite far from the critical point and thus, if real, would have to be attributed to a very-low-frequency relaxation process. We did not attempt to do this. We note that our model accounts quite well for the *increase* in this dispersion as the critical point is approached. The second point of disagreement occurs with regard to the attenuation at 1 MHz observed by Fritsch and Carome. Since they did not regard their 1-MHz measurements as being accurate[13] we do not feel that these discrepancies are serious. The third discrepancy lies in the fact that the velocities predicted by the fit at 130 MHz are somewhat above the measured values, which may be an indication that a more elaborate fit is required.

We next inquired as to whether all of the data could be adequately modeled without using any critical contribution to the viscosity. We again used a single relaxation and adjusted b_1 and τ so as to obtain agreement with $\omega \mathrm{Im} b(\omega)$, which is determined primarily by the sound speed as a function of frequency. This was possible; however, the resulting fit failed to account properly for the 36-MHz attenuation near the critical point. Figures 2 and 3 show the sound speed and attenuation per wavelength calculated from the fit involving a critical contribution, using the exact dispersion equation, and some of the actual data points given in the references from which the smoothed data in Table I were extracted.

We can compare the values of f_τ needed to fit the data with the values which would be expected on the basis of low-frequency, low-pressure ultrasonic studies of vibrational relaxation in SF_6.[24,25] The fundamental relaxation time τ_0 is 0.70×10^{-6} sec at 1 atm and 45°C, while it is 0.68×10^{-6} sec at 55°C. In the case of CO_2 this time has been found to scale very accurately with density,[26,27] $\rho\tau_0$ being constant to densities greater than the critical density at a temperature of 50.6°C, which is ~20°C above T_c. Since at 1 atm the density of SF_6 between 45 and 55°C is 5.6×10^{-3} g/cm^3, while

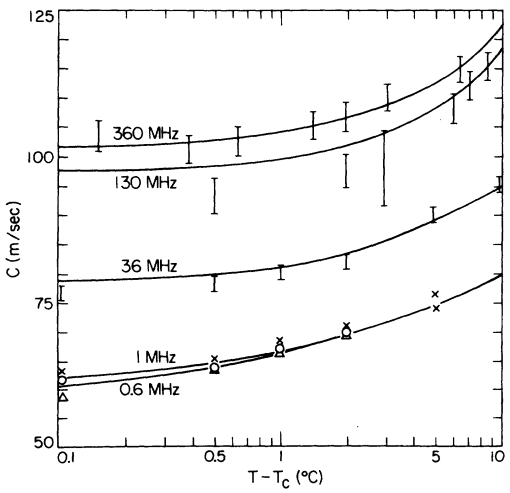

FIG. 2. Experimental and theoretical values of the sound speed C in m/sec. The 2-kHz data points are represented by triangles, the 0.6-MHz data by open circles, and the 1-MHz data by crosses.

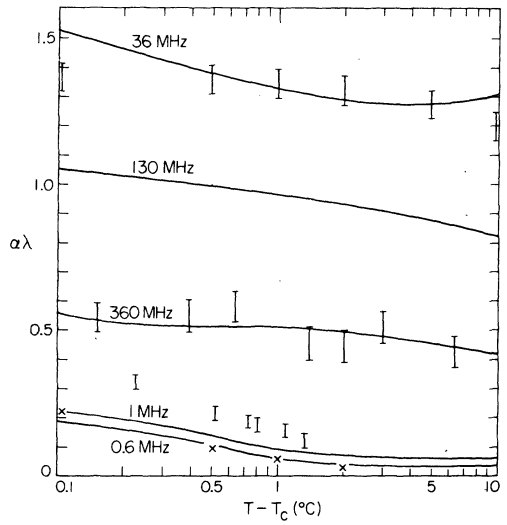

FIG. 3. Experimental and theoretical values of the attenuation per wavelength $\alpha\lambda$. The 0.6-MHz data are represented by crosses.

the critical density is 0.737 g/cm^3, the fundamental relaxation time for the exchange of energy with the vibrational states should be 5.1×10^{-9} sec in this temperature range at the critical density. This time is related to the value of τ, describing the relaxation in sound propagation, through the relation[28]

$$\tau=\tau_0\left(\frac{C_V-C'}{C_V}\right), \tag{19}$$

where C' is the heat capacity of the vibrational states. The quantity C' can be calculated quite accurately using the Planck-Einstein equation[24]

$$C'=R\sum_i g_i\left(\frac{h\nu_i}{k_BT}\right)^2\frac{e^{h\nu_i/k_BT}}{(e^{h\nu_i/k_BT}-1)^2}, \tag{20}$$

where g_i is the degeneracy of the ith level, ν_i its frequency, h is Planck's constant, and R is the gas constant. For SF_6, C' is 0.47×10^7 erg/g°C at 45°C and 0.48×10^7 erg/g°C at 55°C. Using these values of C' and the values of C_V listed in Table IV we calculated the expected relaxation frequency as a function of temperature, and the results are shown in the last line of Table III. The decrease in the expected relaxation frequency as $T\to T_c$ is due solely to the accompanying increase in C_V. The fact that the value of f_τ required to fit the data is constant at 75 MHz may indicate that a consistent treatment of the problem would require considering both the critical relaxation and that due to the internal states as being coupled, so that, for example, the heat capacity appearing in the prefactor d should be relaxed at higher frequencies where the heat capacity of the vibrational states is frozen out.

Although it is less meaningful to calculate values of b_1 from the values of C', since the presence of another relaxation affects these values, we should expect agreement away from the critical point, where the critical relaxation processes play no role. We have calculated b_1 at every temperature, using the relation[29]

$$b_1=C_0^2\left(1-\frac{1}{\gamma}\right)\frac{C'}{C_V-C'}, \tag{21}$$

which holds for the case of a single relaxation, and these values are shown in the last line of Table II. Both the values of b_1 and the expected relaxation frequencies are quite sensitive to the values of C_V far from T_c. For example, if at $T-T_c=5$°C the true value of C_V were lower than the table value by 8%, this would increase the expected value of b_1 to 71×10^6 cm^2/sec^2 and would also increase the expected relaxation frequency to 77 MHz, bringing both values into excellent agreement with the parameters used in the fit. An error of 8% in C_V is completely reasonable at $T-T_c=5$°C. Since the value of C_V at $T-T_c=10$°C was obtained by extrapolation and may well be in error by considerably more than 8% no meaning should be ascribed to the decrease in the calculated values of b_1 and f_τ at this temperature. It is clear, however, that the expected decrease in b_1 as $T\to T_c$ is not reflected in the values of b_1 actually required to fit the data. To some extent this should be expected, since the presence of another relaxation process has the effect of increasing the values of b_1.[30] In fact it is possible to use the calculated values of b_1 and f_τ to fit the data, provided that the heat capacity appearing in the prefactor d is allowed to relax with the frequency dependence of a single relaxation at the expected value of f_τ. Although we find this fact intriguing we feel that the use of this more complicated model is not justified by our present theoretical understanding of critical behavior in a fluid possessing internal degrees of freedom.

*This research was supported by the National Science Foundation, under Grant No. GH34420.
†Alfred Sloan Foundation Fellow.
‡Present address: Xerox Corp., Rochester, New York.

[1]E. I. Gordon and M. G. Cohen, Phys. Rev. 153, 201 (1967).
[2]L. P. Kadanoff and J. Swift, Phys. Rev. 166, 89 (1968).
[3]K. Kawasaki, Phys. Rev. A 1, 1750 (1970).

[4]D. S. Cannell, Ph.D. thesis (Physics Department, Massachusetts Institute of Technology, 1970) (unpublished).
[5]D. S. Cannell and G. B. Benedek, Phys. Rev. Lett. 25, 1157 (1970).
[6]C. W. Garland, D. Eden, and L. Mistura, Phys. Rev. Lett. 25, 1161 (1970).
[7]D. Eden, C. W. Garland, and J. Thoen, Phys. Rev. Lett. 28, 726 (1972).
[8]P. E. Mueller, D. Eden, C. W. Garland, and R. C. Williamson, Phys. Rev. A 6, 2272 (1972).
[9]H. Z. Cummins and H. L. Swinney, Phys. Rev. Lett. 25, 1165 (1970).
[10]D. Eden and H. L. Swinney (to be published).
[11]R. Mohr, K. H. Langley, and N. C. Ford, Jr., J. Acoust. Soc. Am. 49, 1030 (1971).
[12]W. G. Schneider, J. Chem. Phys. 18, 1300 (1950); Can. J. Chem. 29, 243 (1951); J. Chem. Phys. 20, 759 (1952).
[13]K. Fritsch and E. F. Carome, NASA Contractor Report NASA CR-1670, 1970 (unpublished).
[14]R. Mohr and K. H. Langley, J. Phys. (Paris) Suppl. 33, C1-97 (1972).
[15]D. Sarid and D. S. Cannell, Rev. Sci. Instrum. (to be published).
[16]S. R. De Groot and D. Mazur, *Non-Equilibrium Thermodynamics* (North-Holland, Amsterdam, 1963), p. 316.
[17]H. L. Swinney, in *Photon Correlation and Light Beating Spectroscopy*, Proceedings of the NATO Ad-Study Institute, edited by H. Z. Cummins and E. R. Pike (Plenum, New York, 1973).
[18]L. D. Landau and E. M. Lifshitz, *Statistical Physics* (Addison-Wesley, Reading, Mass., 1958), pp. 51 and 52.
[19]G. T. Feke, G. A. Hawkins, J. B. Lastovka, and G. B. Benedek, Phys. Rev. Lett. 27, 1780 (1971).
[20]V. G. Puglielli and N. C. Ford, Jr., Phys. Rev. Lett. 25, 143 (1970).
[21]W. H. Mears, E. Rosenthal, and J. V. Sinka, J. Phys. Chem. 73, 2254 (1969).
[22]J. H. Lunacek and D. S. Cannell, Phys. Rev. Lett. 27, 841 (1971).
[23]E. S. Wu, Ph.D. thesis (Materials Science Center, Cornell University, 1973) (unpublished).
[24]C. L. O'Conner, J. Acoust. Soc. Am. 26, 361 (1959).
[25]R. Holmes and M. A. Stoti, Brit. J. Appl. Phys. 1, 1331 (1968).
[26]M. C. Henderson and L. Peselnick, J. Acoust. Soc. Am. 29, 1074 (1957).
[27]M. C. Henderson and J. Klose, J. Acoust. Soc. Am. 31, 29 (1959).
[28]K. F. Herzfeld and T. A. Litovitz, *Absorption and Dispersion of Ultrasonic Waves* (Academic, New York, 1959), p. 82.
[29]Reference 28, Eq. 12-7.
[30]Reference 28, Sec. 20–22.